科学通报 2018 年 第 63 卷 第 9 期：846 ~ 855

论 文

《中国科学》杂志社
SCIENCE CHINA PRESS

四川盆地西南缘 PETM 事件的环境磁学记录

杨会会[1,2]，申琪[3]，冉亚洲[3]，李传志[3]，梁文天[3]，袁四化[4]，靳春胜[1,5*]

1. 中国科学院地质与地球物理研究所新生代地质与环境实验室，北京 100029;
2. 中国科学院大学，北京 100049;
3. 西北大学大陆动力学国家重点实验室，西安 710069;
4. 防灾科技学院地震科学系，廊坊 065201;
5. 中国科学院青藏高原地球科学卓越创新中心，北京 100101

* 联系人，E-mail: csjin@mail.iggcas.ac.cn

2017-11-13 收稿，2018-02-01 修回，2018-02-02 接受，2018-03-21 网络版发表

中国科学院 A 类战略性先导科技专项“泛第三极环境变化与绿色丝绸之路建设”、国家重大科学研究计划(2013CB956403)和国家自然科学基金(41672200, 41421002)资助

摘要 四川盆地西南缘的前陆盆地中保存了巨厚的新生代沉积，是研究青藏高原东南缘地区气候和构造演化的重要地质记录. 本文通过对四川盆地西南缘新生代沉积物进行年代学、环境磁学和碳同位素的综合研究，发现了在陆相沉积中报道甚少的古新世-始新世极热(Paleocene-Eocene Thermal Maximum, PETM)事件. 多项高分辨率的环境磁学参数曲线可同已报道的海陆相碳同位素曲线进行良好对应，揭示了PETM事件详细的演化过程，表明环境磁学参数可以作为反映古近纪温暖气候事件的替代性指标. 在机制上，PETM时期大气中CO_2含量剧增导致全球增温，局部中低纬度地区降水量增加. 首先，降水量增加导致源区化学风化增强，加速了硅酸盐中Fe^{2+}的析出并转化成亚铁磁性矿物，使得PETM时期地层中亚铁磁性矿物富集. 其次，降水量增加导致河流水动力增强，缩短了碎屑物质中亚铁磁性矿物的氧化时间，使其未完全风化至赤铁矿便被沉积，导致该时期地层中亚铁磁性矿物含量的增加以及多项环境磁学指标异常. 通过环境磁学手段揭示的PETM事件，进一步丰富了该事件的全球陆相地质记录，为研究其演化过程和机制提供了新的视角.

关键词 古新世-始新世极热事件(PETM)，环境磁学，四川盆地，碳同位素，古新世-始新世

深海氧同位素记录显示，全球气候自进入新生代以来发生了显著的变化，主要表现为由两极无冰盖的温暖气候转变为两极有冰盖的冰室气候[1]. 在新生代全球气候变冷的大趋势下，地球仍存在几次较为突出的全球性暖事件，其中较为显著的古新世-始新世极热事件(Paleocene-Eocene Thermal Maximum, PETM)，曾引起全球气候的剧烈变化. 该事件最先报道于大洋钻孔研究中[2]，后又在陆相地质记录中不断被发现[3~7]. PETM事件是发生在古新世-始新世界线附近的一次全球温度及全球CO_2浓度快速增加的事件. PETM期间大气中CO_2增加的总量可与人类开始大规模利用化石燃料以来及预期使用所释放的总量对比[8,9]，因而在地质记录中以显著的碳同位素负漂为特征[1~7]. PETM期间中纬内陆和其他地区都存在4~5℃的增温[9,10]，伴随有降水量增加、水循环加快等气候现象[10~14]. 在陆地上有大量新的物种出现，包括奇蹄类、偶蹄类、啮齿类和灵长类动物[15]. 在海洋生态系统中，由于海底缺氧导致大量底栖有孔虫灭绝[1,16,17].

作为新生代以来板块构造活动最为强烈的地区，

引用格式：杨会会，申琪，冉亚洲，等. 四川盆地西南缘 PETM 事件的环境磁学记录. 科学通报, 2018, 63: 846–855
Yang H H, Shen Q, Ran Y Z, et al. Environmental magnetic records of PETM in the southwestern Sichuan Basin (in Chinese). Chin Sci Bull, 2018, 63: 846–855, doi: 10.1360/N972017-01192

青藏高原在隆升的过程中形成了大量的沉积盆地. 这些盆地广泛分布于青藏高原周缘及其腹地, 包含了丰富的构造和古气候信息, 备受学界的关注[18~20], 是研究PETM事件潜在的重要区域. 前人对青藏高原周缘盆地开展了诸多研究, 尤其以东北缘的研究程度较高[18~20], 但均无PETM相关的报道. 青藏高原东南缘龙门山南段前陆盆地的古近纪沉积较为完整且出露良好[21~24], 具备记录PETM事件的可能. 因此, 本研究选取龙门山南段前陆盆地的古近纪陆相沉积地层作为研究对象, 在四川省天全县始阳镇建立始阳剖面. 该剖面厚742 m, 岩性以棕红-紫红泥质粉砂岩和粉砂质泥岩为主.

1 区域地质环境

研究区位于青藏高原东缘四川盆地西缘龙门山断裂南段(图1), 平均海拔约800 m, 现代年均温度为14.1~17.9℃, 年降水量约1700 mm, 属于亚热带季风气候. 始阳剖面(102°50′52.789″E, 30°0′26.575″N)位于芦山-始阳向斜的东南部边缘, 在天全县城东南方向约12 km处(图1).

川西盆地晚白垩世以来的沉积地层局限在盆地的西南部, 属于龙门山山前冲积扇, 表现为楔状地质体, 是对龙门山南段褶皱冲断构造的响应[22,23]. 从中-新生代沉积迁移和构造转换来看, 龙门山断裂带白垩纪-古近纪的前缘凹陷在本地区发育, 反映了印度与亚欧板块碰撞在川西地区的沉积和构造响应[24]. 研究区内晚白垩世以来的沉积地层由老到新依次为晚白垩统天马山组K_2t、夹关山组K_2j、灌口组K_2g和古近系名山组E*m*、芦山组E*l*以及上覆第四系沉积物Q. 其中, 古近系以滨湖相和浅湖相沉积为主. 始阳剖面下部的沉积物粒度向上变细, 单层沉积厚度递减, 岩性由砂渐变为泥, 反映了沙坪向泥坪沉积的转变. 剖面中部主要沉积杂色泥岩, 为浅湖相沉积环境. 剖面上部主要为泥岩、粉砂质泥岩和粉砂岩互层, 为浅湖和泥坪交替沉积相(图2(a)). 此外, 由于龙门山山前冲积扇的部分物源是三叠纪海相碳酸盐沉积, 所以研究区沉积地层中碳酸盐碎屑沉积较为普遍[21,26].

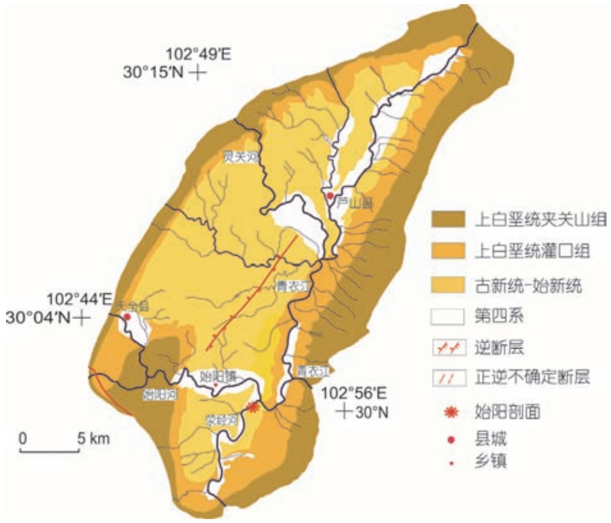

图1 研究区地质简图(据四川省地质局区域地质调查图[25]修改)以及始阳剖面位置

Figure 1 Geological map of the studied area and the location of the Shiyang section (marked by a red star). This map was modified from regional geological survey of Bureau of Geology of Sichuan Province[25]

介形类生物在白垩纪至古近纪最为繁盛, 物种丰富、分布广泛, 可在较大空间范围内进行对比分析, 因而物种特征普遍具有较强的时代意义. 前人研究表明: 在四川盆地西南地区天马山组中, 介形类组合以*Jingguella*及其各亚属和*Deyangia*的发育为特征, 指示地层沉积年代为早白垩世; 在本区夹关山组上部及灌口组中, 介形类以*Cristocypridea-Quadracypris-Limnocythere paomagangensis-Cypridea Pseudocypridina*构成组合, 其时代属于晚白垩世; 在名山组的上部产出*Sinocypris funingensis-Limnocythere hubeiensis-Ilyocypris dungshanensis*组合, 其时限为始新世[27]; 在芦山地区的芦山组中, *Pinnocypris postacuta-Limnocythere jiangsuensis-Cyprinotus formalis*组合出现的频率较高, 属始新世至渐新世[27,28].

2 材料和方法

本研究沿剖面按地层年代由新到老采集了2套实验样品, 包括用于古地磁定年的定向柱样、用于获取环境磁学、岩石磁学及碳同位素信息的离散样品. 我们用便携式手持汽油钻机钻取了354块古地磁定向柱样, 然后用双刀片切割机加工成2.2 cm高的标准测试柱样. 自室温开始以10~50℃的温度间隔, 对这些样品采用MMTD48热退磁炉开展系统热退磁至685℃, 利用2G-760低温超导磁力仪测量每一步退磁后样品的天然剩磁强度. 所有退磁实验均在零磁空间(<300 nT)完成(详细的磁性地层学结果将另文发表).

本文共采集了离散样品761个, 用于多项磁学参数的测量. 首先对这些样品采用卡帕桥旋转磁化率仪以976 Hz的频率进行了低频磁化率测量, 进行质量归

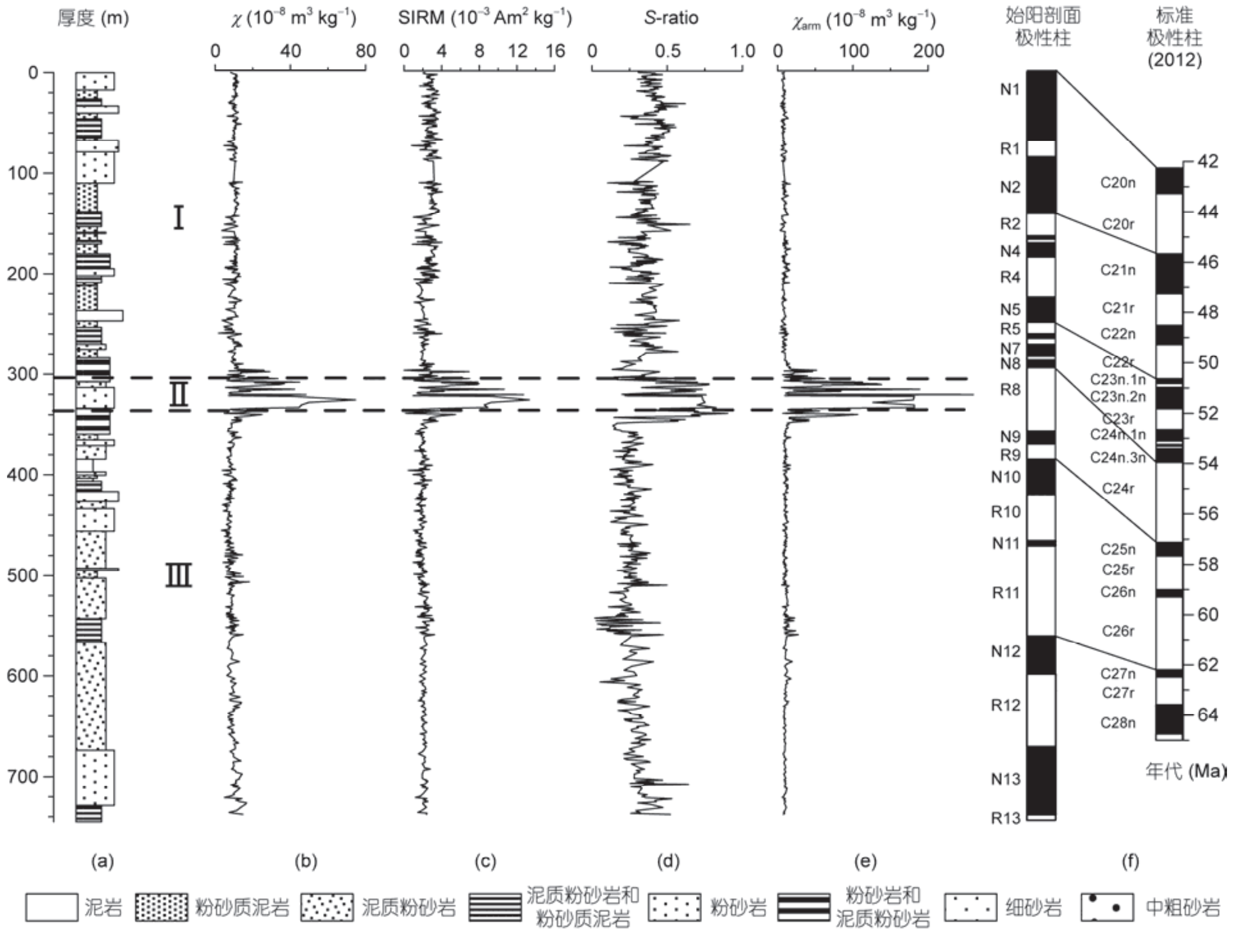

图 2 始阳剖面岩性柱(a)各项环境磁学参数((b)~(e))和磁性地层(f). (a) 地层Ⅰ, Ⅱ和Ⅲ段用虚线划分, 其范围分别为 0~305, 305~340 和 340~742 m; (b) χ表示低频磁化率; (c) SIRM是施加 2.3 T的磁场后测得的饱和等温剩磁; (d) *S*-ratio=IRM$_{-300\ \mathrm{mT}}$/SIRM, 其值代表样品中低矫顽力磁性矿物的含量; (e) χ_{arm}表示非磁滞剩磁磁化率; (f) 磁极性序列. 标准极性柱(2012)引自Gradstein等人[37], 始阳剖面详细的磁性地层结果将另文发表

Figure 2 Lithostratigraphic column (a), magnetic parameter sequences ((b)–(e)) and magnetostratigraphy results (f) of the Shiyang section. The dashed lines divide the section into three segments. (a) Segment Ⅰ, Ⅱ and Ⅲ are at 0–305, 305–340 and 340–742 m of the Shiyang section respectively; (b) χ is mass-specific magnetic susceptibility of samples; (c) SIRM was imparted in a 2.3 T field; (d) *S*-ratio=IRM$_{-300\ \mathrm{mT}}$/SIRM. IRM$_{-300\ \mathrm{mT}}$ was imparted at 0.3 T by reversing the orientation of the samples; (e) χ_{arm}: ARM was imparted in a 100 mT alternating field with a 0.05 mT direct field. χ_{arm} was calculated from the ARM which is normalized using the bias field. (f) The geomagnetic polarity timescale (GPTS) of Gradstein et al.[37]. The detailed results of magnetostratigraphy of the Shiyang section will be published elsewhere

一化得到质量磁化率χ. 通过对样品加2.3 T磁场后采用磁力仪测量得到饱和等温剩磁(saturation isothermal remanent magnetization, SIRM). 通过反转样品在脉冲磁化率仪中的位置, 对其施加0.3 T的磁场后可测得IRM$_{-300\ \mathrm{mT}}$, 由此得到*S*-ratio(=IRM$_{-300\ \mathrm{mT}}$/SIRM), 用以指示样品中低矫顽力磁性矿物的含量[29,30]. 非磁滞剩磁(anhysteretic remanent magnetization, ARM)在100 mT的交流磁场和0.05 mT的直流偏转场中测得, 利用直流偏转场进行归一化后得到非磁滞剩磁磁化率值χ_{arm}. χ_{arm}的值在磁性矿物种类上与样品中的亚铁磁性矿物成正相关, 在磁畴状态上与样品中单畴(SD)或者小的假单畴(PSD)含量成正相关[31].

基于上述实验, 我们挑选了8个样品分别进行了磁滞回线Hysterestic Loop和磁化率随温度变化曲线κ-*T*的测量. Loop的测量采用MicroMag3900振荡磁力仪进行. κ-*T*曲线采用带有CS-4高温炉的MFK1-FA卡帕桥磁化率仪测量, 从室温到700℃的加热过程在氩气环境中进行, 以减少氧化对实验结果造成的影响. 以上实验均在中国科学院地质与地球物理研究所古地磁实验室完成.

此外, 我们在环境磁学参数异常层段挑选了13个样品进行碳酸盐无机碳同位素测量. 分析方法采用磷

酸法，流程如下：取一定量研磨好的样品在真空条件下与100%纯磷酸盐在70℃下反应2 h生成CO_2气体并收集．用MAT-252型稳定同位素气体质谱仪测定CO_2的$\delta^{13}C$值，其分析精度为±0.2‰，结果以VPDB标准表示．该测试在中国科学院地球环境研究所完成．

3 结果

3.1 环境磁学参数

根据始阳剖面的环境磁学结果，可将地层分为3段(图2(b)~(e))．地层Ⅰ与Ⅲ段的χ值较低且基本一致，平均值为9.64×10^{-8} m^3 kg^{-1}，SIRM和χ_{arm}值也较低且S-Ratio值基本维持在0.4，表明地层中主要磁性矿物为高矫顽力的反铁磁性矿物，磁畴状态可能以大的PSD，MD或二者的混合为主[31~36]．而Ⅱ段存在明显的χ峰，峰值可达74.64×10^{-8} m^3 kg^{-1}；SIRM峰值指示了该段样品SP/SD界线以上的亚铁磁性矿物浓度增加[29,30]；S-Ratio峰值表明Ⅱ段富含低矫顽力的亚铁磁性矿物；χ_{arm}表现出异常高值，可能指示该段SD的亚铁磁性矿物的含量增加[31]．

由上述环境磁学结果可知地层Ⅰ与Ⅲ段磁性矿物主要以大PSD或MD磁畴状态的高矫顽力磁性矿物为主，而地层Ⅱ段的样品中则富含SD或小PSD磁畴状态的亚铁磁性矿物．

3.2 岩石磁学结果

利用磁性矿物的磁滞回线可以识别磁性矿物的种类[29,30,38]．地层Ⅱ段样品的磁滞回线特征与Ⅰ和Ⅲ段样品的结果存在显著差别．首先，Ⅱ段样品均呈现出细长而陡直的形状且几乎都在400 mT时饱和，其饱和磁化强度值(M_s)为2.93×10^{-2}~6.12×10^{-2} Am^2 kg^{-1} (图3(e)~(h))，远高于Ⅰ和Ⅲ段样品，指示了样品以低矫顽力的亚铁磁性矿物为主，例如磁铁矿[29,30]．对比而言，Ⅰ和Ⅲ地层样品则表现为明显的蜂腰状，指示亚铁磁性和反铁磁性矿物的混合特征[39,40]．并且，这些样品的饱和磁场强度远高于Ⅱ段样品，如图3(a)和(b)样品在1.5 T时仍未饱和，这表明Ⅰ和Ⅲ段的样品中含有更多的高矫顽力的反铁磁性矿物，与前文环境磁学揭示的各段磁性矿物特征一致．

在κ-T曲线的加热过程，所有样品的磁化率值在580℃附近都存在明显的降低，并在600~700℃之间进一步降低至0，指示样品中含有磁铁矿和赤铁矿．对于地层Ⅰ与Ⅲ段的样品，温度上升到580~600℃时，样品的磁化率值较初始值降低了50%~60%(图4(a)~(d))，

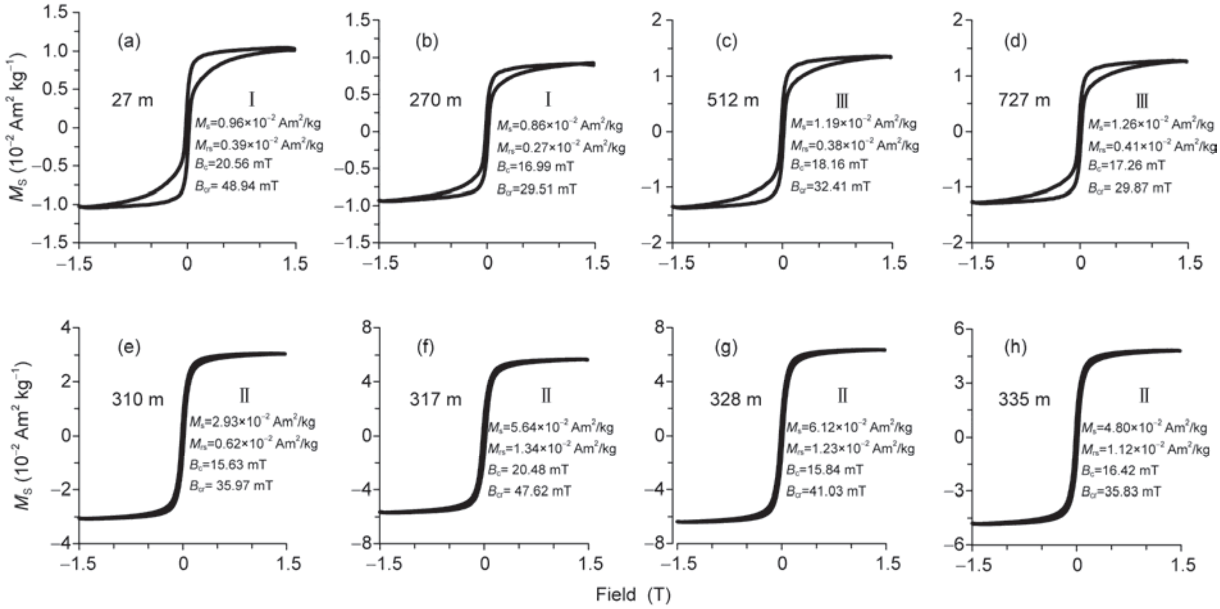

图 3 始阳剖面代表性样品磁滞回线(经过顺磁校正). M_s，饱和磁化强度；M_{rs}，饱和剩余磁化强度；B_c，矫顽力；B_{cr}，剩磁矫顽力；(a), (b) 样品来自地层Ⅰ；(c), (d) 样品来自地层Ⅲ；(e)~(h) 样品来自地层Ⅱ段

Figure 3 Representative magnetic hysteresis loops (after slope correction) for samples from the Shiyang section. M_s, saturation magnetization; M_{rs}, saturation remnant magnetization; B_c, coercivity; B_{cr}, remanence coercivity. (a), (b) Segments Ⅰ; (c), (d) segments Ⅲ; (e)–(h) segment Ⅱ

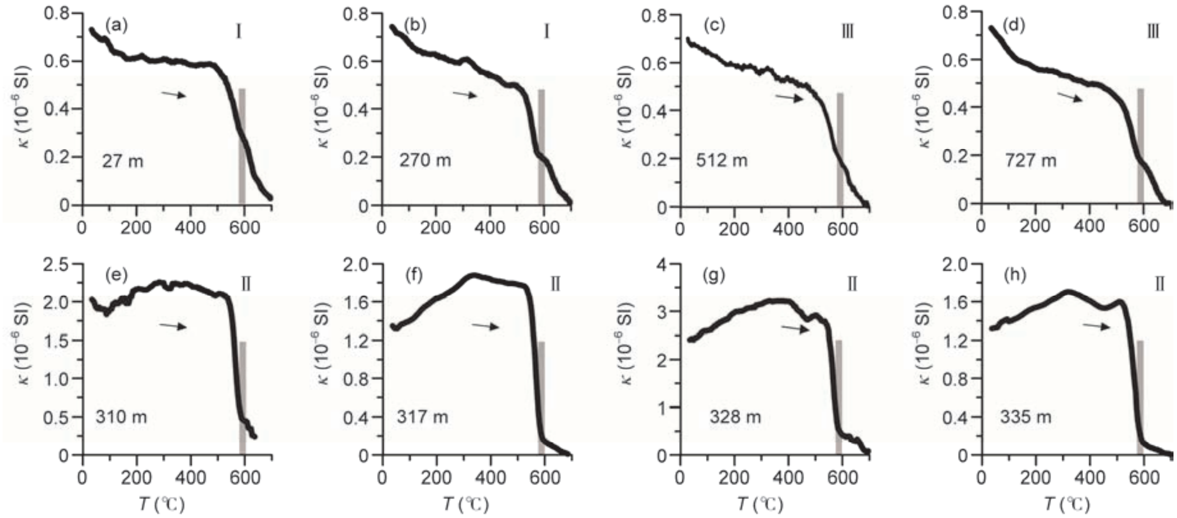

图 4 始阳剖面代表性样品磁化率随温度变化曲线(κ-T). (a), (b) 样品来自地层Ⅰ; (c), (d) 样品来自地层Ⅲ; (e)~(h) 样品来自地层Ⅱ段

Figure 4 Representative temperature-dependent susceptibility (κ-T) curves of samples from the Shiyang section. (a), (b) Segments Ⅰ; (c), (d) segments Ⅲ; (e)–(h) segment Ⅱ

在600~700℃之间仍经历了大幅度降低. 由于赤铁矿磁化率显著低于磁铁矿, 图4(a)~(d)的κ-T曲线清晰地表明地层Ⅰ与Ⅲ段的样品中含有大量的赤铁矿. 而地层Ⅱ段的样品(图4(e)~(h)), 其磁化率值在约580℃已经下降至初始值的10%左右(图4(e)~(h)), 说明其主要磁性矿物为磁铁矿, 仅有少量赤铁矿存在.

另外, 随温度升高至300℃时, 地层Ⅱ段样品的磁化率值存在明显的上升趋势, 这可能是由该温度段SP/SD磁性矿物颗粒受热解阻所致[34](图4(e)~(h)). 在300~450℃, 磁化率值逐步降低, 这通常被认为是由亚稳态的磁赤铁矿受热分解为赤铁矿所致[41,42](图4(e)~(h)). 随后在540℃左右出现了一个小的峰值, 可能是受样品中磁铁矿颗粒解阻效应的影响(图4(e)~(h)). 综上所述, 地层Ⅰ和Ⅲ段样品中磁性矿物以赤铁矿为主, 地层Ⅱ段以磁铁矿和磁赤铁矿为主.

3.3 碳同位素结果

碳同位素结果在图5(a)中展示, 从剖面342 m的地层处开始迅速负漂(−3‰), 在330 m处漂至−7.5‰后在324 m处回返至−4‰, 之后在近10 m厚的地层中(322~312 m)又持续负漂至−10‰, 到达本剖面最大负漂值, 随后在304 m处回返至−5‰, 再次负漂至−8‰(300 m处)后开始缓慢回返, 在280 m处回返至−4‰, 整个负漂过程结束.

4 讨论

4.1 始阳剖面PETM事件的确定

PETM事件最先发现于海洋钻孔ODP 690B中, 之后陆续报道于海陆地质记录, 表现为该时期全球大气中的CO_2含量剧增, 全球温度增高, 在地质记录中以碳同位素大幅度负漂为特征[1~7]. 图2显示磁性地层极性柱的R8对应于标准极性柱的C24r, 地层Ⅱ段的年代界于55.7~54.3 Ma[30], 与其他PETM研究的磁性地层年代较为一致[3,6].

Zhu等人[7]在中国华中地区南阳盆地发现了记录于碳酸岩中的PETM事件, 并将其碳同位素曲线与钻孔ODP 690B和美国Bighorn盆地的碳同位素曲线进行了对比分析, 认为可以将这3条碳同位素曲线的异常波动归纳为a~i共9个阶段(图5(f)~(h)). 本文环境磁学参数较好地限制了该事件, 与南阳盆地、ODP 690B钻孔和美国Bighorn盆地的碳同位素曲线之间具有良好的对比关系.

图5所示的始阳剖面各项环境磁学参数中, 345~337 m的峰值及回落, 可与碳同位素曲线负漂阶段a及其回返后的阶段b形成对比; 在337~321 m处的环境磁学参数峰值对应了碳同位素曲线中快速负漂的阶段c和e, 及其中间相对稳定的阶段d, 且该段地层中各项环境磁学参数值的显著降低可能与碳同位素曲线中的快速回返阶段f对应; 在321~312 m处, 各个

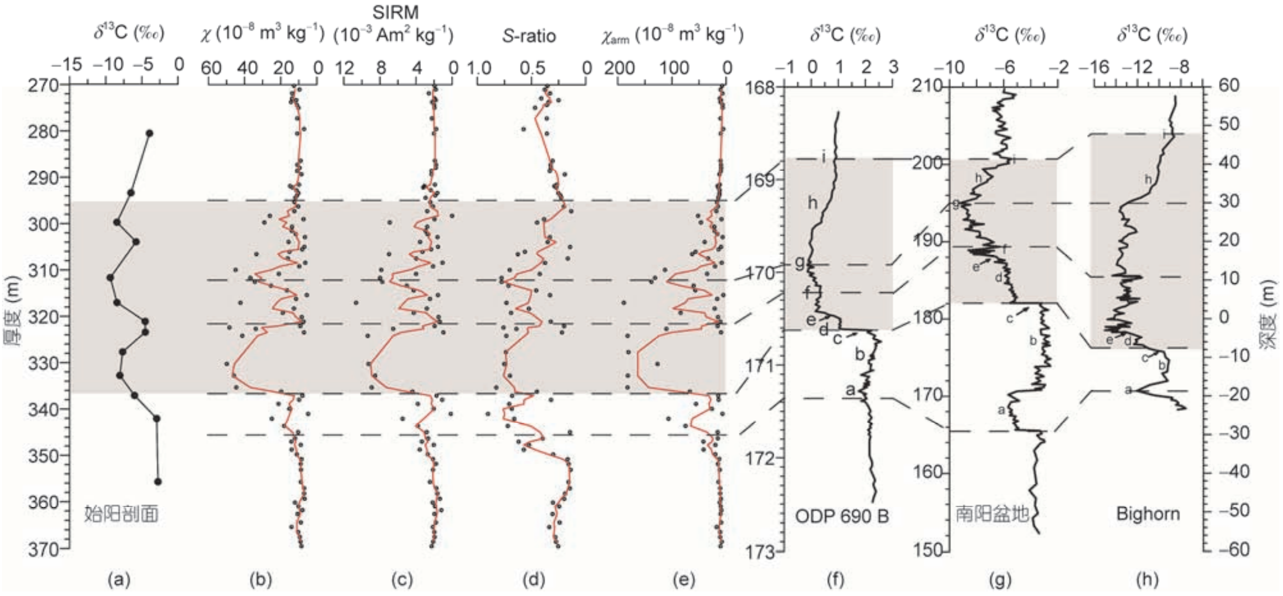

图 5 始阳剖面 270~370 m的碳同位素结果与环境磁学参数和其他海陆相碳同位素记录的对比. (a) 始阳剖面的碳同位素曲线; (b) 低频磁化率曲线; (c) 饱和等温剩磁曲线; (d) 软磁性矿物比值; (e) 非磁滞剩磁磁化率曲线; (f) ODP 690B的碳同位素曲线[2]; (g) 南阳盆地的碳同位素曲线[3]; (h) Bighorn的碳同位素曲线[7]. 阴影表示PETM范围; (f)~(h)中的a~i指Zhu等人[7]对PETM碳同位素负漂划分的 9 个不同阶段

Figure 5 Results of carbon isotope and parameters of environmental magnetism at 270–370 m interval of the Shiyang section, and their comparison to the other carbon isotope records. (a) Carbon isotope records of the Shiyang section; (b) χ; (c) SIRM; (d) *S*-ratio; (e) χ_{arm}; (f) carbon isotope curves of ODP 690B[2]; (g) carbon isotope curves of Nanyang Basin[3]; (h) carbon isotope curves of Bighorn Basin[7]. The grey shadows indicate the PETM; (f)–(h) letters a–i are nine different phases of the PETM divided by Zhu et al.[7]

参数的增强可与缓慢负漂的阶段g对比；在312~297 m处，剖面上所有磁学参数缓慢降低与阶段h和i碳同位素的逐渐回返趋势一致，反映了PETM事件的结束(图5(b)~(h)).

综上所述，本文环境磁学参数较好地限制了PETM事件，同时，图5(a)揭示本研究的碳同位素曲线与其他PETM记录的碳同位素结果形态上总体相似. 因此，我们认为本剖面地层Ⅱ段记录了PETM事件.

始阳剖面环境磁学约束的PETM持续地层厚度约40 m，仅次于美国Bighorn盆地PETM事件的地层厚度. 由于磁性地层年代学框架的粗略性，本文难以给出始阳剖面PETM具体过程的准确时限，需进一步开展高分辨率的古气候替代性指标测试，识别PETM期间所含的轨道周期，从而精确约束其演化过程.

4.2 环境磁学参数异常的机制

前文实验结果表明地层Ⅱ段的磁性矿物以SD的亚铁磁性矿物为主，而Ⅰ和Ⅲ段的磁性矿物以赤铁矿为主. 因此，地层Ⅱ段磁学参数异常可能反映了其沉积时期的区域环境突变. 该变化可能受沉积物源、搬运过程和成岩作用等因素影响[19,31,32].

前人对龙门山南段前陆盆地的分析，表明白垩纪以来盆地沉积相和古流向未发生显著变化. 自中生代以来，龙门山一直是川西南地区陆相前陆盆地的主要物源区[43]. 同时，本剖面为浅湖-滨湖沉积岩相，沉积物主要为高度氧化的泥岩-砂岩红层，未见沉积后溶解作用. 因此，始阳剖面环境磁学参数变化的主要原因可能是流域向盆地输入磁性矿物颗粒的含量和类型发生了变化.

众多研究表明PETM时期地球中低纬度的气温和湿度增加，水循环加快[10,13,14]. 对美国Wyoming地区植物群落的研究表明，在PETM期间美国中纬内陆地区的气温升高了5℃左右[10]. 孢粉学证据也揭示在PETM时期，印度次大陆降水量增加气候湿润，热带雨林的范围扩大[13]. 来自南半球的黏土矿物证据同样表明，在PETM时期降水量增加，气候变得湿润[14]. 因此，可以认为在PETM时期，本文研究区气候相较之前更为湿润，降水量增加.

从硅酸盐质和硫酸盐质母岩中分解释放出的铁可形成一系列的含铁矿物，这些矿物在不同的气候环境中通过不同的途径发生变化[44]. 从母岩中风化出的铁离子，通过某种方式合成磁铁矿或者水铁矿，

磁铁矿沿着磁铁矿-磁赤铁矿-赤铁矿的路径进一步氧化，最终形成赤铁矿[45~47]．水铁矿遵循水铁矿-磁赤铁矿-赤铁矿的路径转化[45~47]．在水铁矿向赤铁矿转化过程中，中间产物的磁性矿物粒径随着时间不断增长，从SP变为SD[48]．

始阳剖面在地层Ⅰ和Ⅲ段沉积时，冲积扇河流的水动力较弱，导致所携物质的搬运时间较长，使原岩中分解出来的含铁矿物在搬运过程中经历较长时间的氧化，有充分的时间完成水铁矿/磁铁矿-赤铁矿的转化过程，因此在地层Ⅰ和Ⅲ段中沉积物以赤铁矿为主．而在地层Ⅱ段沉积时，即PETM时期研究区降水量的增加对源区风化和搬运沉积过程都会造成影响．一方面，区域降水量增加可导致化学风化增强，加速了母岩碎屑中铁离子的析出和亚铁磁性矿物的快速生成．Boyle等人[49]根据模拟结果认为，在一定时间内(<0.1 Ma)，风化增强促使含铁硅酸盐释放Fe^{2+}并快速转化成为亚铁磁性矿物．Dearing等人[50,51]的研究也表明，降水量增加可以促进水解作用的发生和含铁矿物的风化，从而促进次生磁铁矿物的生成．另一方面，降水量增加导致河流的水动力和搬运能力增强，缩短了碎屑物质的氧化时间，使得原岩中的磁性矿物未完成磁铁矿/磁赤铁矿向赤铁矿的转化便被搬运至沉积区埋藏，在地层中表现为载磁矿物以SD的亚铁磁性矿物为主．因此，地层Ⅱ段的环境磁学参数显著异常于地层Ⅰ和Ⅲ段．

前人在其他地区的研究曾运用水动力强度-搬运时间-氧化程度的机制来解释地层中环境磁学参数的变化．在风化过程中，原岩中的磁铁矿转化为磁赤铁矿，氧化晚期进一步生成赤铁矿[52]．原岩碎屑暴露在氧化环境中的时间越长，其被氧化的程度越高．Fang等人[19]通过对西宁盆地始新世-中新世河湖相沉积物的研究，提出了低温氧化假说．他们认为环境较为湿润时，区域河流水动力增强，源区碎屑物质在搬运过程中受低温氧化作用的时间相对较短．碎屑物质沉积后所处的浅湖环境，也阻止了其沉积后的进一步氧化，该过程导致了地层中的赤铁矿含量较低而亚铁磁性矿物含量较高．

综合而言，我们认为PETM期间降水量增加导致了源区风化增强，促使含铁硅酸盐释放Fe^{2+}并转化成为亚铁磁性矿物．同时河流搬运能力增强，导致碎屑物质在亚铁磁性矿物阶段即被搬运埋藏．这两个过程共同引起了始阳剖面PETM期间地层的环境磁学参数异常．

5 结论

本研究在龙门山前陆盆地发现了陆相沉积中报道甚少的古新世-始新世极热事件(PETM事件)．我们建立了742 m厚的始阳剖面，磁性地层定年结果表明剖面年代为65~42 Ma．在55.7~54.3 Ma附近，多项环境磁学参数表现出显著峰值．岩石磁学结果表明在此期间，沉积物中含有更多的亚铁磁性矿物，而在其他时段则以反铁磁性矿物为主．通过对比表明，本研究环境磁学结果与已报道的PETM事件碳同位素结果有较好的对应关系．本剖面的碳同位素结果在该层段表现为明显的负漂移，最大值达到10‰，验证了环境磁学反映的信息．综合而言，我们认为高精度的环境磁学指标可以作为反映古近纪温暖气候事件的替代性指标之一．在此基础上，我们对本剖面的环境磁学异常做出了机制上的解释．在PETM事件期间，一方面，降水增加使得源区含铁硅酸盐风化增强，加速了Fe^{2+}的析出并转化为亚铁磁性矿物．另一方面，研究区降水量增加，使得河流水动力和搬运能力增强，碎屑物质中的亚铁磁性矿物未来得及氧化成赤铁矿，便被迅速搬运至沉积区埋藏．我们认为上述两个原因联合导致了PETM期间地层中亚铁磁性矿物增多，多项环境磁学参数异常．

致谢 感谢审稿人和编辑老师对本文提出的宝贵意见．

参考文献

1 Zachos J C, Pagani M, Sloan L, et al. Trends, rhythms, and aberrations in global climate 65 Ma to present. Science, 2001, 292: 686–693

2 Knennet J P, Scott L D. Abrupt deep-sea warming palaeoceanographic changes and benthic extinctions at the end of the Palaeocene. Nature, 1991, 353: 225–229

3 Koch P L, Zachos J C, Dettman D L. Stable isotope straitgraphy and paleoclimatology of the Paleogene Bighorn basin (Wyoming, USA).

Paleogeogr Paleoclimatol Paleoecol, 1995, 115: 61–89

4 Bowen G J, Clyde W C, Koch P L, et al. Mammalian dispersal at the Paleocene/Eocene boundary. Science, 2002, 295: 2062–2065

5 Harrington G J, Clechenko E R, Kelly D C. Palynology and organic-carbon isotope ratios across a terrestrial Palaeocene/Eocene boundary section in the Williston basin, North Dakota, USA. Paleogeogr Paleoclimatol Paleoecol, 2005, 226: 214–232

6 Bowen G J, Koch P L, Meng J, et al. Age and correlation of fossiliferous late Paleocene-early Eocene strata of the Erlian basin, inner Mongolia, China. Amer Mus Novit, 2005, 3474: 34–74

7 Zhu M, Ding Z, Wang X, et al. High-resolution carbon isotope record for the Paleocene-Eocene Thermal Maximum from the Nanyang basin, central China. Chin Sci Bull, 2010, 55: 3606–3611

8 IPCC. Climate Change 2007: The Physical Science Basis. Cambridge: Cambridge University Press, 2007. 1–996

9 Chen Z L, Ding Z L. A review on the Paleocene-Eocene Thermal Maximum (in Chinese). Quat Res, 2011, 31: 937–950 [陈祚伶，丁仲礼. 古新世-始新世极热事件研究进展. 第四纪研究, 2011, 31: 937–950]

10 Wing S L, Harrington G J, Smith F A, et al. Transient floral change and rapid global warming at the Paleocene-Eocene boundary. Science, 2005, 310: 993–996

11 Winguth A, Shellito C, Shields C, et al. Climate response at the Paleocene-Eocene Thermal Maximum to greenhouse gas forcing—A model study with CCSM3. J Clim, 2010, 23: 2562–2584

12 Egger H, Homayoun M, Huber H, et al. Early Eocene climatic, volcanic, and biotic events in the northwestern Tethyan Untersberg section, Austria. Paleogeogr Paleoclimatol Paleoecol, 2005, 217: 243–264

13 Prasad V, Farooqui A, Tripathi S K M, et al. Evidence of late Palaeocene-early Eocene equatorial rain forest refugia in southern western Ghats, India. J Biosci, 2009, 34: 777–797

14 Raigemborn M S, Brea M, Zucol A, et al. Early Paleogene climate at mid latitude in south America: Mineralogical and Paleobotanical proxies from continental sequences in Golfo San Jorge Basin (Patagonia, Argentina). Geol Acta, 2009, 7: 127–147

15 Gingerich P D. Mammalian responses to climate change at the Paleocene-Eocene boundary: Polecat Bench record in the northern Bighorn basin, Wyoming. Geol Soc Am Bull, 2003, 369: 463–478

16 Kaiho K, Arinobu T, Ishiwatari R, et al. Latest Paleocene benthic foraminiferal extinction and environmental changes at Tawanui, New Zealand. Paleoceanography, 1996, 11: 447–465

17 Thomas E, Shackleton N J. The Paleocene-Eocene benthic foraminiferal extinction and stable isotope anomalies. Geol Soc, 1996, 101: 401–441

18 Zhang K X, Wang G C, Ji J L, et al. Paleogene-Neogene stratigraphic realm and sedimentary sequence of the Qinghai-Tibet Plateau and their response to uplift of the plateau. Sci Chin Ser D-Earth Sci, 2010, 53: 1271–1294

19 Fang X M, Zan J B, Appel E, et al. An Eocene-Miocene continuous rock magnetic record from the sediments in the Xining basin, NW China: Indication for Cenozoic persistent drying driven by global cooling and Tibetan Plateau uplift. Geophys J Int, 2015, 201: 78–89

20 Chang H, Li L J, Qiang X K, et al. Magnetostratigraphy of Cenozoic deposits in the western Qaidam basin and its implication for the surface uplift of the northeastern margin of the Tibetan Plateau. Earth Planet Sci Lett, 2015, 430: 271–283

21 Zeng Y F, Ji X T, Li Y L, et al. Sequence stratigraphy analysis of late Cretaceous-Paleogene terrigenous basin in Tianquan Lushan Sichuan (in Chinese). Miner Petrol, 1992, 12: 66–73 [曾允孚，纪相田，李元林，等. 天全芦山地区晚白垩世-早第三纪陆相盆地层序地层分析. 矿物岩石, 1992, 12: 66–73]

22 Lin M B. A brief discussion on the tection evolutional history of terminal region at the south section in Longmen mountain, Sichuan Province (in Chinese). J Chengdu Univ Tech, 1993, 20: 46–51 [林茂炳. 简论龙门山南段末端地区构造发展史. 成都地质学院学报, 1993, 20: 46–51]

23 Liu S G, Luo Z L, Zhao X K, et al. Coupling relationships of sedimentary basin-orogenic belt systems and their dynamic models in west China—A case study of the Longmenshan orogenic belt-west Sichuan foreland basin system (in Chinese). Acta Geol Sin, 2003, 77: 177–186 [刘树根，罗志立，赵锡奎，等. 中国西部盆山系统的耦合关系及其动力学模式——以龙门山造山带-川西前陆盆地系统为例. 地质学报, 2003, 77: 177–186]

24 Chen X Z, Jia D, Wei G Q, et al. Meso-Cenozoic sediment transport and tectonic transition in the western Sichuan foreland basin (in Chinese). Geol China, 2008, 35: 472–481 [陈竹新，贾东，魏国齐，等. 川西前陆盆地中-新生代沉积迁移. 中国地质, 2008, 35: 472–481]

25 Bureau of Geology of Sichuan Province. Regional Geological Survey of Baoxing in Sichuan Province at the Proporational Scale of 1∶200000 (in Chinese). Beijing: Geological Map Printing Factory of China, 1977 [四川省地质局. 中华人民共和国区域地质调查报告宝兴幅（1∶20 万）. 北京：中国地质图制印厂, 1977]

26 Li Y, Zeng Y F. Fill sequence of Longmen mountain foreland basin (in Chinese). J Chengdu Univ Tech, 1994, 21: 46–55 [李勇，曾允孚. 龙门山前陆盆地充填序列. 成都理工学院学报, 1994, 21: 46–55]

27 Wang Q W, Kan Z Z, Liang B, et al. Statigraphic division and correlation of the continental Meso-Cenozoic group in Ya’an west Sichuan basin (in Chinese). Acta Geol Sichuan, 2006, 26: 65–69 [王全伟，阚泽忠，梁斌，等. 四川盆地西部雅安地区陆相中新生代地层划分

及区域对比. 四川地质学报, 2006, 26: 65–69]
28 Yan L, Zhao B, Zhou Y X, et al. The discovery of the Palaeogene strata and their fossil assemblages in the Lushan formation, Lianhe region, Hongya, Sichuan (in Chinese). Sediment Geol Tethyan Geol, 2014, 34: 38–43 [严亮, 赵兵, 周羽漩, 等. 四川洪雅联合地区芦山组地层的发现及生物组合特征. 沉积与特提斯地质, 2014, 34: 38–43]
29 Thompson R, Oldfeild F. Environmental Magnetism. London: Allen and Unwin Ltd, 1986. 1–220
30 Evans M E, Heller F. Evironmental Magnetism: Principles and Applications of Enviromagnetics. Amsterdam: Academic Press, 2003. 1–202
31 Liu Q S, Roberts A P, Larrasoana J C, et al. Environmental magnetism: Principles and applications. Rev Geophys, 2012, 50: RG4002
32 Pan Y X, Zhu R X. The progress of environmental magnetism (in Chinese). Progr Geophys, 1996, 11: 87–99 [潘永信, 朱日祥. 环境磁学研究现状和进展. 地球物理学进展, 1996, 11: 87–99]
33 Bloemendal J, Liu X M. Rock magnetism and geochemistry of two Plio-Pleistocene Chinese Loess-Palaeosol sequences-implications for quantitative palaeoprecipitation reconstruction. Paleogeogr Paleoclimatol Paleoecol, 2005, 226: 149–166
34 Deng C L, Vidic N J, Verosub K L, et al. Mineral magnetic variation of the Jiaodao Chinese loess/paleosol sequence and its bearing on long-term climatic variability. J Geophys Res, 2005, 110: B03103
35 Maher B A. Magnetic properties of some synthetic sub-micron magnetites. Geophys J, 1988, 94: 83–96
36 Liu Q S, Banerjee S K, Jackson M J, et al. Grain sizes of susceptibility and anhysteretic remanent magnetization carriers in Chinese loess/paleosol sequences. J Geophys Res, 2004, 109: B03101
37 Gradstein F M, Ogg J G, Schmitz M D, et al. The Geologic Time Scale 2012. Oxford: Elsevier Publications, 2012. 855–921
38 Dunlop D J, Ozdemir O. Rock Magnetism. Cambridge: Cambridge University Press, 1997. 1–565
39 Roberts A P, Verosub K L. Wasp-waisted hysteresis loops: Mineral magnetic characteristics and discrimination of components in mixed magnetic systems. J Geophys Res-Solid Earth, 1995, 100: 17909–17924
40 Deng C L, Zhu R X, Verosub K L, et al. Mineral magnetic properties of loess/paleosol couplets of the central Loess Plateau of China over the last 1.2 myr. J Geophys Res-Solid Earth, 2004, 109: B01103
41 Deng C L, Zhu R X, Verosub K L, et al. Paleoclimatic significance of the temperature-dependent susceptibility of Holocene loess along a NW-SE transect in the Chinese Loess Plateau. Geophys Res Lett, 2000, 27: 3715–3718
42 Florindo F, Zhu R X, Guo B, et al. Magnetic proxy climate results from the Duanjiapo Loess section, southern most extremity of the Chinese Loess Plateau. J Geophys Res-Solid Earth, 1999, 104: 645–659
43 Peng J, Chen H D, Zeng Y F. Characteristics and provenance analysis of the Mesozoic and Cenozoic sandstone in the foreland basin of the south part of Longmenshan Mountain (in Chinese). Region Geol China, 2000, 19: 77–84 [彭军, 陈洪德, 曾允孚. 龙门山南段前陆盆地中-新生代砂岩特征及物源分析. 中国区域地质, 2000, 19: 77–84]
44 Cornell R M, Schwertmann U. The Iron Oxides: Structure, Properties, Reactions, Occurrence and Uses. Weinheim, New York: Elsevier Science Ltd, 1996. 1–573
45 Barron V, Torrent J, Grave E D. Evidence for a simple pathway to maghemite in Earth and Mars soils. Geochim Cosmochim Acta, 2002, 66: 2801–2806
46 Cabello E, Morales M P, Serna C J, et al. Magnetic enhancement during the crystallization of ferrihydrite at 25 and 50°C. Clays Clay Miner, 2009, 57: 46–53
47 Barron V, Torrent J, Grave E D. Hydromaghemite, an intermediate in the hydrothermal transformation of 2-line ferrihydrite into hematite. Am Miner, 2003, 88: 1679–1688
48 Liu Q S, Barrón V, Torrent J, et al. Magnetism of intermediate hydromaghemite in the transformation of 2-line ferrihydrite into hematite and its paleoenvironmental implications. J Geophys Res, 2008, 113: B01103
49 Boyle J F, Dearing J A, Blundell A, et al. Testing competing hypotheses for soil magnetic susceptibility using a new chemical kinetic model. Geol Soc Am, 2010, 38, 12: 1059–1062
50 Dearing J A, Hay K L, Babon S M J, et al. Magnetic susceptibility of soil: An evaluation of conflicting theories using a national data set. Geophys J Int, 1996, 127: 728–734
51 Dearing J A, Livingstone I P, Bateman M D, et al. Palaeoclimate records from OIS 8.0–5.4 recorded in loess-palaeosol sequences on the Matmata Plateau, southern Tunisia, based on mineral magnetism and new luminescence dating. Quat Int, 2001, 76-77: 43–56
52 Sidhu P S. Transportation of trace element-substituted maghemite to hematite. Clay Miner, 1988, 36: 31–38

Summary for "四川盆地西南缘 PETM 事件的环境磁学记录"

Environmental magnetic records of PETM in the southwestern Sichuan Basin

Huihui Yang[1,2], Qi Shen[3], Yazhou Ran[3], Chuanzhi Li[3], Wentian Liang[3], Sihua Yuan[4] &
Chunsheng Jin[1,5*]

[1] *Division of Cenozoic Geology and Environment, Institute of Geology and Geophysics, Chinese Academy of Sciences, Beijing 100029, China;*
[2] *University of Chinese Academy of Sciences, Beijing 100049, China;*
[3] *State Key Laboratory of Continental Dynamics, Northwest University, Xi'an 710069, China;*
[4] *Department of Earthquake Science, Institute of Disaster Prevention, Langfang 065201, China;*
[5] *Center for Excellence in Tibetan Plateau Earth Sciences, Chinese Academy of Sciences, Beijing 100101, China*
* Corresponding author, E-mail: csjin@mail.iggcas.ac.cn

Collision between the Indian and Eurasian plates produced concomitant uplift of the Tibetan Plateau and its basin-ridge geomorphological systems. As the world's largest and highest plateau, Tibetan Plateau surface relief has significant dynamic and thermal effects on atmospheric circulation and on regional and global climate. Large numbers of Cenozoic sedimentary basins that developed concomitantly in and around the Tibetan Plateau are attributed to intracontinental deformation and Tibetan Plateau uplift due to India-Eurasia collision, such as the Sichuan Basin which is located in the eastern margin of the Tibetan Plateau. During the Cenozoic, the Sichuan Basin has received thick sediments which provide us an excellent opportunity to reconstruct the tectonic and climatic evolution of the southeastern Tibetan Plateau areas. In this study, we present results from a long sedimentary sequence (thick of 742 m) at Shiyang section (102°50′E, 30°0′N) from the southwestern Sichuan Basin. Magnetostratigraphic sequences were constructed for Shiyang section which dates the Mingshan Formation to ~65–42 Ma. Mass-specific low field magnetic susceptibility (χ), anhysteretic remanent magnetization (ARM) and isothermal remanent magnetization (IRM) sequences of 761 bulk samples were measured at the Paleomagnetism Laboratory of the Institute of Geology and Geophysics, Chinese Academy of Sciences, Beijing. Thus, χ_{arm} and S-ratio can be calculated. These environmental magnetism sequences display that there is a distinct peak in the stratigraphic interval 340–305 m. Eight samples were selected for detailed rock magnetism including temperature-dependent susceptibility (κ-T) curves and hysteresis loops. Rock magnetism results display that samples from the 340–305 m interval are dominated magnetically by magnetite and maghemite particles. However, magnetic minerals are dominated by hematite particles for samples outside of the 340–305 m interval. Inorganic carbon isotope results of the selected 13 samples display that there exist some distinct negative shifts of carbon isotope values in the 340–305 m interval. The maximum negative shift can reach −10‰. Combining results of geochronology, environmental magnetism and carbon isotope of Cenozoic deposits from the Shiyang section, we can define that the PETM (Paleogene-Eocene Thermal Maximum) palaeoclimatic event was recorded in the 340–305 m interval at Shiyang section. Discovery of the PETM in the Sichuan Basin enriches the PETM records in the world's terrestrial sediments and provides a new view to reveal its processes and mechanism.

The various curves of high-resolution environmental magnetism in the 340–305 m interval are comparable to results of the reported carbon isotope from other terrestrial and marine sediments, such as the Nanyang Basin in China, the Bighorn Basin in USA, and the ODP 690B core in Antarctica Ocean. This indicates that environmental magnetism sequences in this study can be used as reliable palaeoclimatic proxies to unveil the PETM. After learning more geoscience records and the paleoenvironment conditions they reveal in different areas in the world during the PETM, we suppose that the peak values of the environmental magnetism sequences in this study were attributed to increased palaeoprecipitation during the PETM period. Firstly, increased precipitation led to chemical weathering enhancement and facilitated the decomposition of silicate minerals and separation of Fe^{2+} which could quickly transfer into ferromagnetic minerals. Secondly, increased precipitation also contributed to enhanced hydrodynamic force of rivers. This accelerated the depositional processes of the clastic materials and shortened the oxidization time of magnetic debris. It may be another reason for the increased content of ferromagnetic minerals in the stratigraphic interval of PETM. Therefore, changes in environmental magnetic curves could be linked with the detailed process of the PETM.

Paleocene-Eocene Thermal Maximum (PETM), environmental magnetism, Sichuan Basin, carbon isotope, Paleocene-Eocene

doi: 10.1360/N972017-01192